Controlling electron localization in H_2^+ by intense plasmon-enhanced laser fields

I. Yavuz,[1] M. F. Ciappina,[2] A. Chacón,[3] Z. Altun,[1] M. F. Kling,[2,4] and M. Lewenstein[3,5]
[1]*Marmara University, Physics Department, 34722 Ziverbey, Istanbul, Turkey*
[2]*Max-Planck-Institut für Quantenoptik, Hans-Kopfermann-Strasse 1, D-85748 Garching, Germany*
[3]*Institut de Ciéncies Fotóniques, The Barcelona Institute of Science and Technology, 08860 Castelldefels (Barcelona), Spain*
[4]*Department of Physics, LMU Munich, Am Coulombwall 1, D-85748 Garching, Germany*
[5]*Instituciò Catalana de Recerca i Estudis Avançats, Lluis Companys 23, 08010 Barcelona, Spain*
(Received 19 November 2015; published 3 March 2016)

We present a theoretical study of the H_2^+ molecular ion wave-packet dynamics in plasmon-enhanced laser fields. These fields may be produced, for instance, when metallic nanostructures are illuminated by a laser pulse of moderated intensity. Their main property is that they vary in space on a nanometric scale. We demonstrate that the spatial inhomogeneous character of the plasmonic fields leads to an enhancement of electron localization (EL), an instrumental phenomenon to control molecular fragmentation. We suggest that the charge imbalance induced by the surface-plasmon resonance near the metallic nanostructure is the origin of the increase in the EL.

DOI: 10.1103/PhysRevA.93.033404

I. INTRODUCTION

Studies of atomic and molecular quantum dynamics configure the body of interests in contemporary atomic, molecular, and optical physics. There are various ways to induce such dynamics, but a very distinct one is to expose the atomic or molecular systems to an intense and coherent electromagnetic radiation. As a consequence of this coupling, new and diverse phenomena occur. Among the plethora of processes which take place, the two most prominent ones are the high-order harmonic generation (HHG) and the above-threshold ionization (ATI). They both lie at the core of the so-called attosecond physics [1,2]. The quasiclassical picture of these two phenomena relies on the commonly named three-step or simple man's model [3,4]. Briefly, this approach can be summarized listing the subsequent steps: (i) tunnel ionization due to an intense and low-frequency laser field, (ii) acceleration of the free electron by the laser electric field, and (iii) recollision with the parent ion after the temporally oscillating laser electric field reverses the direction of the electronic motion. In HHG the electron recombines with the remaining ion core and the excess of energy is converted into a high-energy photon [2]. On the other hand, if the electron is rescattered by the atomic potential, it gains even more kinetic energy and contributes to the high-energy region of the ATI spectrum [5].

Commonly, the laser ionization process is understood by invoking the quasistatic tunnel ionization picture. In this approach in every time (short) interval the laser electric field is considered as a static electric field. This assumption is valid for low photon frequencies—long wavelengths—and the atomic or molecular electron is considered to quickly tunnel out through the barrier created by the combined potentials of the laser electric field and the attractive Coulomb atomic or molecular potential. The main consequence of this description is that the ionization rate presents a maximum whenever the barrier becomes the thinnest, which correlates with the electric-field maxima. This prediction appears to be also valid in the so-called nonadiabatic tunnel ionization, i.e., when the laser electric field is considered to change significantly, while the electron is escaping from the attractive potential of the atomic or molecular core. For these cases the ionization rate exhibits a single maximum during each half cycle of the laser electric-field oscillation [6].

When molecules are used as driven media, the above cited assumptions should be revised, considering that there can be multiple bursts of ionization within a half cycle of the laser electric field [7,8]. By using different numerical models and simulations, it was confirmed that these bursts are related to the effect of transient electron localization (EL) at one of the heavy nuclei of the molecule on a sub-fs time scale [9–11]. Generally, a subcycle oscillation of the electron density occurs after the molecular ion has been stretched to intermediate internuclear distances, and it is due to a trapping of the electron population in a pair of commonly named charge-resonance (CR) states [12,13]. For the case of a simple H_2^+ molecular ion, they are the energetically lowest σ_g and σ_u states. It is likely, however, that both the multiple ionization bursts and the CR show up in other more complex molecules as well. Additionally, EL appears to be responsible for the strongly enhanced ionization rate observed for stretched molecules beyond its equilibrium internuclear separation [14]. Moreover, it was shown that EL can be manipulated, jointly with the control of photoabsorption or photodissociation, by using different alignment techniques [15], or by modifying the laser pulse parameters [16–19].

In the theoretical modeling of conventional strong laser-matter interaction, the main assumption is that both the laser electric field $E(\mathbf{r},t)$ and its associated vector potential $A(\mathbf{r},t)$ are spatially homogeneous in the region where the electron develops its motion and only their time dependence is considered, i.e., $E(\mathbf{r},t) = E(t)$ and $A(\mathbf{r},t) = A(t)$. This is a legitimate assumption since the fields change at most on the scale of the wavelength (800–3000 nm), while the typical size of a laser focus is between several tens to a couple of hundred microns (10^{-6} m). These scales have to be compared with the size of the electronic ground states (typically in the Angstroms (10^{-10} m) range) and the size of the conventional electron excursions, estimated classically using $\alpha = E_0/\omega_0^2$, where E_0 is the peak amplitude of the laser electric field and ω_0 is the laser central frequency; even these sizes remain subwavelength and do not reach more

than several tens of nm (10^{-9} m), for longer wavelengths and higher laser intensities. The latter conclusion comes from the fact that $\alpha \propto E_0\lambda_0^2$, where λ_0 is the wavelength of the driven laser and $E_0 = \sqrt{I}$, I being the laser intensity [2]. In contrast, the fields generated using surface plasmons are spatially dependent on a nanometric scale. By exploiting the surface-plasmon resonance (SPR), locally enhanced electric field can be induced around gold bow-tie nanoantennas. The enhanced field boosts up the low incoming laser intensity, specified in the 10^{11}-W cm^{-2} range, by more than 30 dB, which becomes then strong enough to exceed the threshold laser intensity for XUV generation in noble gases [20–23]. The pulse repetition rate, typically in the MHz domain, remains unaltered without any extra pumping or cavity attachment, configuring one of the main advantages of this setup. From a theoretical viewpoint, plasmonic fields open a wide range of possibilities to enhance and/or shape the spectral and spatial properties of the incoming field [24–27]. A peculiar property of these plasmonic fields is that the enhanced laser electric field is not spatially homogeneous in the region where the electron dynamics takes place, typically delimited by the electronic excursion α. Consequently, significant changes in the laser-matter processes arise.

There has been a remarkable theoretical activity on this subject recently [28–60]. In most of the contributions, however, only the HHG and ATI processes in atoms were studied and analyzed exclusively. Only recently investigations of HHG in the simplest molecule, i.e., H_2^+, driven by plasmonic fields were presented [61,62]. In the present paper we focus on the question of to what extent plasmonic fields could configure a novel and reliable tool to control molecular dynamics, and in particular the EL (for a recent review about the progress in the control of electron dynamics in molecules see e.g. [63]). As mentioned above, these fields are spatially inhomogeneous and thus they offer a new degree of control, which could help us to obtain an even more precise manipulation of the electron and molecular dynamics at a subcycle time scale.

Our paper is organized as follows. In Sec. II, we describe the theoretical methods, including a brief description about the setup that could be utilized for the generation of plasmonic enhanced fields and their main characteristics. Once we have defined our theoretical model and observables of interest, we then analyze them and discuss their properties and implications in Sec. III. Finally, in Sec. IV, we end the paper with conclusions and a brief outlook.

II. METHODOLOGY

A. Field enhancement by the nanostructure

A typical setup including both the metal bow-tie nanoantenna and the driven H_2^+ molecule is shown in Fig. 1 (for more details about the fabrication see, e.g., [20]). The metal nanostructure takes the form of two triangular-shaped pads made of gold with a gap between their apexes (top panel). A planar substrate with a dielectric constant $\epsilon_s = 2.0$ supports them. In the diagram, h is the height, t is the thickness of the metal, and g defines the gap between the tips. In the present simulations, we use $h = 100$ nm, $t = 40$ nm, and $g = 20$ nm. We note that the chosen geometry parameters of the nanoantennas do not correspond to an optimum field

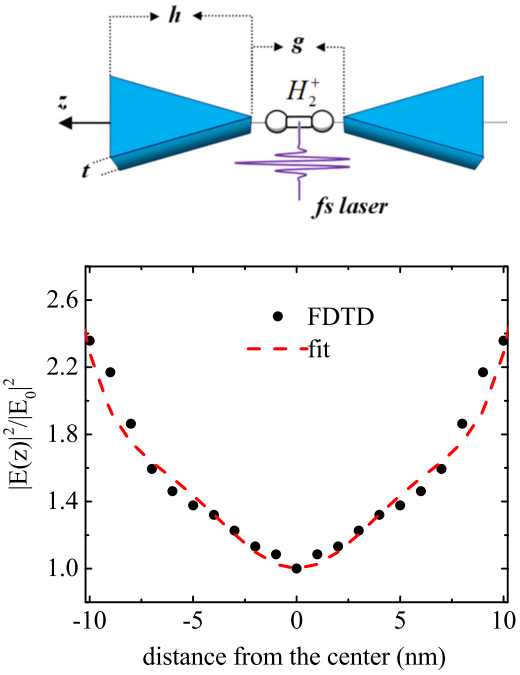

FIG. 1. Top: Typical geometry parameters of the bow-tie shaped gold nanoantennas considered in our study. Here, we take $h =$ 100 nm, $t = 40$ nm, and $g = 20$ nm. The curvature radii of the tips are taken as 4 nm. The bond distance R of the H_2^+ molecule is visually exaggerated for clarity. Bottom: The spatial profile of the field enhancement in the gap, along the z axis, obtained from FDTD simulations. Circles are the actual enhancement determined by the MEEP code and the red (dashed) line is a polynomial fitting, as described in the text. Note that the laser electric-field peak amplitude is enhanced roughly by a factor of 2.5 near the metals compared with the center value, corresponding to 4 dB of increase in the laser intensity.

enhancement, i.e., the nanoantenna is not fully resonant with the laser wavelength, set at $\lambda = 800$ for the finite-difference time domain (FDTD) simulations (see, e.g., [30]), but these values are found to be sufficient to understand the underlying physics of the wave-packet dynamics of the H_2^+ molecular ion near the metallic nanostructure. In order to mimic more realistic situations, the curvature radii of the tips are set to be 4 nm. The spatial profile of the field enhancement around the bow tie is determined using the MEEP code [64], which is based on the FDTD approach. The field enhancement in the gap along the z axis is shown in the bottom panel of Fig. 1, where the spatial profile is normalized to the intensity enhancement at the center ($z = 0$). We observe that the laser electric-field peak amplitude is enhanced roughly by a factor of 2.5 near the metal tips compared with the center value, corresponding to 4 dB of increase in the laser intensity.

B. Numerical solution of the time-dependent Schrödinger equation for the H_2^+ molecule

The numerical solution of the time-dependent Schrödinger equation (TDSE) for the interaction of a linearly polarized laser field with a H_2^+ molecule, in reduced dimensions, can be written as (throughout the paper we employ atomic units

unless otherwise stated)

$$i\frac{\partial}{\partial t}\Psi(z,R,t) = \left[-\frac{1}{2}\frac{\partial^2}{\partial z^2} - \frac{1}{2\mu_p}\frac{\partial^2}{\partial R^2} + V_e(z,R) + V_n(R) + V_L(z,t)\right]\Psi(z,R,t), \quad (1)$$

where $\mu_p = m_p/2$ is the reduced mass of the two nuclei, with m_p the proton mass. In Eq. (1), the potentials $V_e(z,R)$ and $V_n(R)$ are the electron-nuclei attraction and nucleus-nucleus repulsion terms, respectively. The explicit forms of these potentials in reduced dimensions are given below [65]:

$$V_e(z,R) = -\frac{a}{\sqrt{(z+R/2)^2+b(R)}} - \frac{a}{\sqrt{(z-R/2)^2+b(R)}}, \quad (2)$$

and

$$V_n(R) = \frac{1}{R}. \quad (3)$$

In Eq. (2) $a = 0.251$ is a scaling parameter and $b(R)$ is a function introduced to exactly reproduce the three-dimensional potential-energy curve of the $1\sigma_g$ state of the H_2^+ molecule. The laser-molecule interaction term $V_L(z,t)$ in the dipole approximation can be written as

$$V_L(z,t) = -zE(z,t) = -zE(t)[1 + s\kappa(z)], \quad (4)$$

where it is assumed that the laser electric field $E(z,t)$ is now a function explicitly of both time and space. In Eq. (4) $\kappa(z) = \Sigma_i c_i z^i$ is a polynomial series that represents the functional form of the plasmonic field, determined by fitting it to the data obtained from FDTD simulations (see Fig. 1, bottom panel) and s is a switch function taking values $s = 0,1$. s is used to turn the field inhomogeneity on or off, as discussed later. Note that the internuclear axis of the H_2^+ molecule is placed as to coincide with the axis passing through the edges of the nanostructure element (see Fig. 1, top panel). This assumption will be relaxed later (see the Results section).

The field-free form of Eq. (1), i.e.,

$$\left[-\frac{1}{2}\frac{\partial^2}{\partial z^2} - \frac{1}{2\mu_p}\frac{\partial^2}{\partial R^2} + V_e(z,R) + V_n(R)\right]\Psi(z,R) = E\Psi(z,R), \quad (5)$$

is numerically solved based on the Born-Oppenheimer (BO) approximation. When we apply the BO approximation to Eq. (5), its solution is expressed as follows:

$$\Psi(z,R,t=0) = \phi_e(z,R)\psi_n(R), \quad (6)$$

where $\phi_e(z,R)$ is a set of electronic wave functions for fixed values of R and $\psi_n(R)$ is the nuclear wave function. Both $\phi_e(z,R)$ and $\psi_n(R)$ are calculated from the eigenvalue equations

$$\left[-\frac{1}{2}\frac{\partial^2}{\partial z^2} + V_e(z,R)\right]\phi(z,R,t) = E_e(R)\phi(z,R,t) \quad (7)$$

and

$$\left[-\frac{1}{2\mu_p}\frac{\partial^2}{\partial R^2} + E_e(R) + V_n(R)\right]\psi(R) = E\psi(R), \quad (8)$$

respectively.

The field-free solutions of Eqs. (7) and (8) for H_2^+ give an equilibrium bond distance $R = 2.0$ a.u. The ionization potential I_p at the equilibrium $1\sigma_g$ state is found to be $|E_e(R = 2.0)| = 30.0$ eV, i.e., the actual value I_p of the H_2^+ molecule is indeed reproduced.

The time-dependent part of the laser electric field in Eq. (4) is taken as $E(t) = E_0 f(t)\cos(\omega_0 t)$. E_0 and ω_0 are the peak amplitude [E_0 (a.u.) $= \sqrt{I/I_0}$ and $I_0 = 35.1$ PW cm^{-2}] and the frequency of the driving laser electric field, respectively. $f(t)$ is a flat-top ten-cycles-long pulse envelope with half-cycle ramp up or down (the total time duration is 27 fs for a laser wavelength $\lambda = 800$ nm). During the simulations both the electronic and nuclear wave functions are multiplied by mask functions of the form $\cos^{1/8}$ in each time step in order to avoid spurious reflections at the boundaries [66].

By using the time-dependent wave function $\Psi(z,R,t)$ of Eq. (1) it is then possible to compute a set of physical quantities of interest, namely, (i) the time-dependent norm $N(t)$,

$$N(t) = \int_0^\infty dR \int_{-\infty}^\infty dz |\Psi(z,R,t)|^2, \quad (9)$$

(ii) the ionization probability $P_{\rm ion}(t)$,

$$P_{\rm ion}(t) = 1 - N(t), \quad (10)$$

(iii) the dissociation channels through upper $P_+(t)$ or lower $P_-(t)$ nuclei,

$$P_\pm(t) = \int_{R_c}^\infty dR \int_0^{\pm z_c} dz |\Psi(z,R,t)|^2, \quad (11)$$

(iv) the dissociation probability $P_{\rm dissoc}(t)$,

$$P_{\rm dissoc}(t) = P_+(t) + P_-(t), \quad (12)$$

and (v) the asymmetry parameter $A(t)$,

$$A(t) = P_+(t) - P_-(t). \quad (13)$$

The integration limits in Eq. (11) R_c and z_c are taken as 10 a.u. The asymmetry parameter $A(t)$ determines the degree of localization in either of the heavy nuclei upon dissociation. Here, $A(t) > 0$ or $A(t) < 0$ refer to a high degree of localization on the upper or the lower nuclei, respectively. For $A(t) = 0$, the dissociative wave packet is evenly distributed over both nuclei or no dissociation occurs at all.

Finally, the time-dependent expectation value of the internuclear distance $R(t)$ is calculated by the following expression:

$$\langle R(t)\rangle = \frac{1}{N(t)}\int_0^\infty R dR \int_{-\infty}^\infty dz |\Psi(z,R,t)|^2. \quad (14)$$

This quantity allows us to monitor the time dynamics of the molecular dissociation.

III. RESULTS

In this section, we explore the influence of the spatial inhomogeneous character of the plasmonic field on the dissociation and ionization dynamics of the H_2^+ molecular ion by comparing results for both conventional and spatial inhomogeneous fields. As stated otherwise, we consider that the centroid of H_2^+ coincides with the center of the gap of the metallic nanostructure, as shown in Fig. 1, and the molecule

is initially in the ground electronic $1\sigma_g$ and vibrational $v = 0$ states. In our simulations the H_2^+ molecular ion is aligned parallel to the laser polarization. We could employ different laser-induced molecular alignment techniques to reach this situation. For instance, by manipulating adequately the incoming laser pulse, the impulsive alignment approach could be applied (see, e.g., [15] for more details).

Here, one can think of the field spatial inhomogeneity as a potential landscape the strength of which is enhanced as we move away from the gap center to the metallic surfaces (see Fig. 1). In contrast, a homogeneous field is independent of space and, thus, is constant in the region where the electron dynamics takes place. In other words, the plasmonic character of the laser electric field is effective when the wave packet is released from the bound state and spread across distant regions. Accordingly, there is a strong correlation between the ionization rate and the degree of field spatial inhomogeneity. On the other hand, since opposite charges are confined in opposite sides of the nanostructure due to SPR [20], the freed electrons of target atoms or molecules would experience different (repulsive or attractive) forces depending on the direction of the wave packet's propagation.

Figures 2(a)–2(g) show time-dependent wave-packet properties of the H_2^+ molecular ion in a laser field with and without a spatial inhomogeneous character ($s = 0$ and 1, respectively). The laser intensity and wavelength are fixed at $I = 300$ TW/cm^2 (3×10^{14} W/cm^2) and $\lambda = 800$ nm, respectively. First, in Fig. 2(a) we show the time-dependent variation of R, i.e., $\langle R(t) \rangle$. Considering the laser field is switched off at $t = 27$ fs, it is clear that the plasmonic-laser field is effective when the wave packet begins to relax, resulting in a slightly higher bond elongation. It is also evident from Fig. 2(b) that the field inhomogeneity emerges when ionization reaches a certain level (again almost immediately after the laser pulse is over), which is $P_{\text{ion}} \sim 10^{-2}$. In addition, the ionization probability increases roughly by a factor of 2 after reaching a, sort of, limiting value. However, as shown in Fig. 2(c), the dissociation probability is only slightly lower for $s = 1$ (inhomogeneous) than for $s = 0$ (homogeneous), suggesting a more direct electron ionization channel.

Figures 2(d) and 2(e) show the time variation of the nuclear probability density for $s = 0$ and 1, respectively. In the bound region (i.e., for $R < 10$ a.u.), $s = 0$ and 1 present similar profiles, however the dissociation region (i.e., when $R > 10$ a.u.) is slightly more populated in the case of $s = 0$, consistent with Fig. 2(c).

Finally, Figs. 2(f) and 2(g) show the electron-nuclear coordinate maps when the wave packets are relaxed for a sufficient amount of time after the pulse is turned off. Comparing with the homogeneous case, and in the dissociation region, in particular for $R > 14$ a.u., the wave packet is much more localized on both nuclei for the case of the plasmonic field. This is a significant outcome showing the control the plasmonic character of the field has on EL. In order to quantify this last affirmation, using Eq. (13), we find that, after the wave packet is relaxed, the asymmetry parameter is $A = -7.2 \times 10^{-4}$ for $s = 0$ and $A = 1.3 \times 10^{-2}$ for $s = 1$. Thus the asymmetry (localization) for the case of the plasmonic field is roughly 20 times larger (in absolute numbers) than the conventional case.

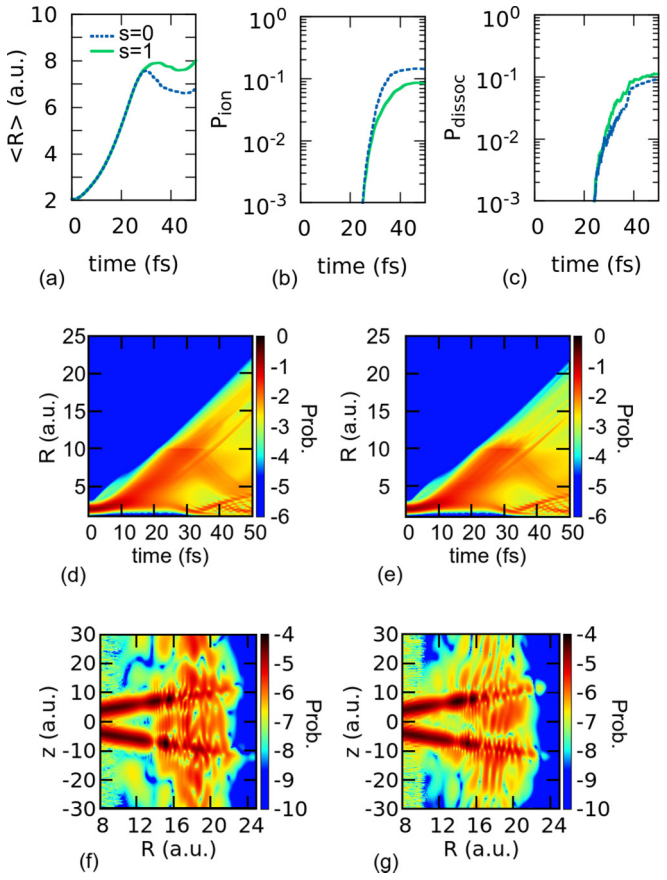

FIG. 2. Top: (a) Temporal variation of R, i.e., $\langle R(t) \rangle$, (b) ionization probability P_{ion}, and (c) dissociation probability P_{dissoc} of the H_2^+ molecule for $s = 0$ (blue dashed lines) and $s = 1$ (green solid lines) [see Eq. (4) for more details]. Center: Time dependence of the R-resolved probability distribution $|\Psi(R,t)|^2$ of H_2^+ for $s = 0$ (left) and $s = 1$ (right). Bottom: (f) and (g) show the snapshots of the wave-packet distributions of $s = 0$ and 1, when the wave packet is relaxed for a sufficient amount of time after the pulse ends. The laser intensity is $I = 300$ TW/cm^2 and $\lambda = 800$ nm. The pulse comprises ten total cycles (27 fs) and we use a flat-top pulse envelope with half-cycle ramp up or down. In panels (d)–(g) the color scale is logarithmic.

The intensity dependence of the *relaxed* asymmetry parameter A of wave-packet dissociation at $\lambda = 800$ and 1600 nm is shown in Fig. 3. For $s = 0$, A is enhanced in the intensity region between 100 and 300 TW/cm^2 for both $\lambda = 800$ and 1600 nm. For weak fields, A is nearly zero due to the low wave-packet dissociation rates. For strong intensities, however, direct wave-packet ionization may occur, which also reduces dissociation. Thus, there is an intermediate intensity region (100–300 TW/cm^2 in our case) such that dissociation reaches a maximum and so is the asymmetry parameter A. On the other hand, comparing with what happens for $\lambda = 800$ nm, A is lower in the intermediate region (100–300 TW/cm^2) for $\lambda = 1600$ nm. This is attributed to faster vibrational motions induced by longer wavelengths, causing an increase in the wave-packet ionization. When the molecule is placed in a plasmon-enhanced laser field ($s = 1$), the asymmetry parameter A is nearly zero in the weak and strong intensity

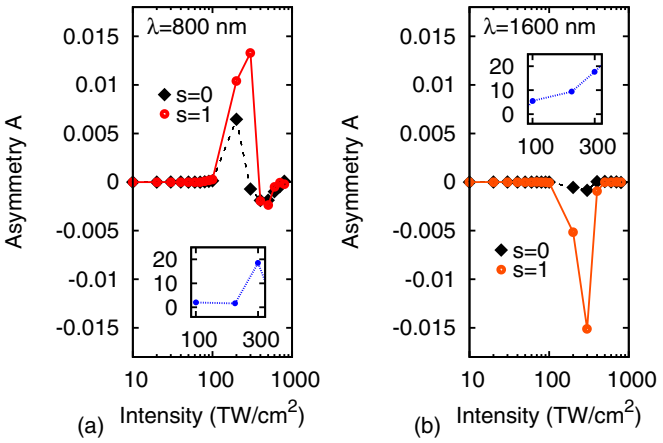

FIG. 3. Variation of the asymmetry parameter ($A = P_+ - P_-$) of H_2^+ as a function of plasmonic field intensity for $s = 0$ (black dashed lines) and $s = 1$ (red solid lines) [see Eq. (4) for details]. A values are calculated after pulse is turned off and then the system is left to relax for a sufficient amount of time. We have performed calculations for two different wavelengths: (a) $\lambda = 800$ nm and (b) $\lambda = 1600$ nm. Insets show the absolute asymmetry parameter enhancement, i.e., the absolute ratio between A of $s = 1$ and 0 (in blue dotted lines), in the region $I = 100$–300 TW/cm^2. The pulse comprises ten total cycles (27 fs for $\lambda = 800$ nm and 54 fs for $\lambda = 1600$ nm, respectively) and we use a flat-top pulse envelope with half-cycle ramp up or down. The spatial profile in both cases is the same as in Fig. 1 (bottom panel).

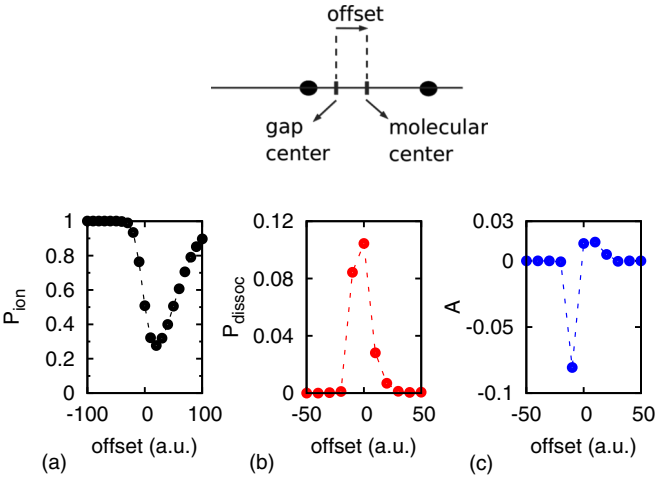

FIG. 4. Top: An illustration showing the gap center of the nanostructure element, molecular center (centroid) of H_2^+, and offset with respect to the gap center. Full circles illustrates the positions of the nuclei. (a) Ionization probability P_{ion}, (b) dissociation probability P_{dissoc}, and (c) asymmetry parameter, $A = P_+ - P_-$, as a function of the centroid offset. P_{ion}, P_{dissoc}, and A are calculated after pulse is turned off and then the system is left to relax for a sufficient amount of time. The laser field parameters are the same as in Fig. 2.

regions, similar to the case of $s = 0$. On the other hand, in the intermediate intensity region, A is dramatically enhanced for both $\lambda = 800$ and 1600 nm. In concrete numbers, for plasmonic fields at $\sim I = 200$–300 TW/cm^2 the asymmetry parameter A is enhanced by a factor of 5–20 compared with the conventional case for both $\lambda = 800$ nm [see Fig. 3(a)] and $\lambda = 1600$ nm [see Fig. 3(b)].

We argue that a charge imbalance, in the nanogap region, induced by the plasmonic field is responsible for the dramatic enhancement in the asymmetry parameter A. So far, we have assumed that the centroid of the molecule and gap center coincides, but in a real experiment we could have molecules randomly distributed in the nanogap region, yet aligned along the z axis. Thus one could ask, what would happen if we displace the molecule from the gap center to the left or right regions along the z axis, where positive or negative charges dominate? In order to gain further understanding in the control of the dissociation asymmetry caused by the plasmonic field, we simulate the wave-packet dynamics of the H_2^+ molecule by displacing its centroid coordinates along the z axis of the nanostructure, as illustrated in Fig. 4 (top). In a region where positive or negative charges dominate, the wave packet might be steered further by attractive or repulsive forces (towards or away from the metallic surface), respectively.

Figures 4(a)–4(c) show the ionization [Fig. 4(a)] and dissociation probabilities [Fig. 4(b)] and the asymmetry parameter A [Fig. 4(c)] as a function of the centroid offset with respect to the gap center. Our results show that there is a clear and strong interplay between ionization, dissociation, and the resulting asymmetry parameter A. The asymmetry in the ionization probability is clearly visible in Fig. 4(a). In the negative offset region, a steep increase in P_{ion} within $-40 <$ offset < 0 a.u. is observed and full ionization occurs beyond this point. In the positive offset region, on the other hand, P_{ion} increases gradually. These results suggest that for the negative offset region the ionized wave packet is pulled towards the metallic surfaces, while in the positive region it is pulled backwards, thus suppressing strongly the ionization probability. After a certain point, however, the wave packet reaches the metallic surface and the electron is absorbed by the metal [28,37].

The wave packet's dissociation probability, P_{dissoc}, in contrast, reaches a maximum for zero offset and gradually diminishes in both regions due to the increase of P_{ion}. The dissociation asymmetry parameter A is larger in the gap center region and maximum, in amplitude, when the offset is ≈ -10 a.u. Positive values of A in the positive offset region and negative values of A in the negative offset region are evident due to an uneven distribution of charges in the nanostructure region. In other words, positive offset is causing EL in the upper nuclei, while the negative offset does so in the lower one, respectively.

IV. CONCLUSIONS AND OUTLOOK

We have studied electron localization (EL) in H_2^+ molecules driven by intense plasmonic fields. These fields are not spatially homogeneous in the region where the electron wave-packet dynamics takes place and, as a consequence, are able to modify substantially the observables. In order to illustrate these facts we have solved the TDSE in reduced dimensions, including both the electron and nuclear dynamics. This model was proven to be suitable for the computation of both electron and nuclear related quantities.

We have shown that the spatial inhomogeneous character of the laser electric field allows us to enhance the localization

of the electron in one of the two protons and given physical grounds for this behavior. This enhancement can be modified, for instance, by engineering the geometry of the metal nanostructure.

Furthermore, with our model we can monitor the dissociation dynamics of the H_2^+ molecule as a function of the position with respect to the center of the gap between the bow ties. This analysis is instrumental in order to perform realistic predictions.

The utilization of plasmonic fields could open the pathway to perform control of the EL and molecular dissociation at a more advanced level.

ACKNOWLEDGMENTS

I.Y. and Z.A. acknowledge support from BAPKO of Marmara University (MU). Calculations are performed at the Simulations and Research Laboratory, Physics Department of MU. A.C. and M.L. acknowledge the Spanish MINECO projects Severo Ochoa (Grant No. SEV-2015-0522) and FOQUS (Grant No. FIS2013-46768-P), the Catalan AGAUR Project No. SGR 874, the European Union Project QUIC, and the European Research Council Project AdG OSYRIS. M.F.K. and M.F.C. are grateful for support by the DFG through the cluster of excellence "Munich Centre for Advanced Photonics".

[1] P. B. Corkum and F. Krausz, Nature Phys. **3**, 381 (2007).
[2] F. Krausz and M. Ivanov, Rev. Mod. Phys. **81**, 163 (2009).
[3] P. B. Corkum, Phys. Rev. Lett. **71**, 1994 (1993).
[4] M. Lewenstein, P. Balcou, M. Y. Ivanov, A. L'Huillier, and P. B. Corkum, Phys. Rev. A **49**, 2117 (1994).
[5] A. de Bohan, P. Antoine, D. B. Milošević, and B. Piraux, Phys. Rev. Lett. **81**, 1837 (1998).
[6] G. L. Yudin and M. Y. Ivanov, Phys. Rev. A **64**, 013409 (2001).
[7] N. Takemoto and A. Becker, Phys. Rev. Lett. **105**, 203004 (2010).
[8] N. Takemoto and A. Becker, J. Chem. Phys. **134**, 074309 (2011).
[9] I. Kawata, H. Kono, and Y. Fujimura, J. Chem. Phys. **110**, 11152 (1999).
[10] F. He, A. Becker, and U. Thumm, Phys. Rev. Lett. **101**, 213002 (2008).
[11] N. Takemoto and A. Becker, Phys. Rev. A **84**, 023401 (2011).
[12] R. S. Mulliken, J. Chem. Phys. **7**, 20 (1939).
[13] L. Pauling, Proc. Natl. Acad. Sci. USA **25**, 577 (1939).
[14] T. Seideman, M. Y. Ivanov, and P. B. Corkum, Phys. Rev. Lett. **75**, 2819 (1995).
[15] H. Stapelfeldt and T. Seideman, Rev. Mod. Phys. **75**, 543 (2003).
[16] V. Roudnev, B. D. Esry, and I. Ben-Itzhak, Phys. Rev. Lett. **93**, 163601 (2004).
[17] F. Anis and B. D. Esry, Phys. Rev. Lett. **109**, 133001 (2012).
[18] T. Rathje, A. M. Sayler, S. Zeng, P. Wustelt, H. Figger, B. D. Esry, and G. G. Paulus, Phys. Rev. Lett. **111**, 093002 (2013).
[19] N. G. Kling, K. J. Betsch, M. Zohrabi, S. Zeng, F. Anis, U. Ablikim, Bethany Jochim, Z. Wang, M. Kbel, M. F. Kling, K. D. Carnes, B. D. Esry, and I. Ben-Itzhak, Phys. Rev. Lett. **111**, 163004 (2013).
[20] S. Kim, J. Jin, Y.-J. Kim, I.-Y. Park, Y. Kim, and S.-W. Kim, Nature (London) **453**, 757 (2008).
[21] M. Sivis, M. Duwe, B. Abel, and C. Ropers, Nature **485**, E1 (2012).
[22] S. Kim, J. Jin, Y.-J. Kim, I.-Y. Park, Y. Kim, and S.-W. Kim, Nature **485**, E1 (2012).
[23] M. Sivis, M. Duwe, B. Abel, and C. Ropers, Nat. Phys. **9**, 304 (2013).
[24] I.-Y. Park, S. Kim, J. Choi, D.-H. Lee, Y.-J. Kim, M. F. Kling, M. I. Stockman, and S.-W. Kim, Nat. Photonics **5**, 677 (2011).
[25] J. Choi, S. Kim, I.-Y. Park, D.-H. Lee, S. Han, and S.-W. Kim, New J. Phys. **14**, 103038 (2012).
[26] N. Pfullmann, C. Waltermann, M. Noack, S. Rausch, T. Nagy, C. Reinhardt, M. Kovačev, V. Knittel, R. Bratschitsch, D. Akemeier *et al.*, New J. Phys. **15**, 093027 (2013).
[27] I.-Y. Park, J. Choi, D.-H. Lee, S. Han, S. Kim, and S.-W. Kim, Ann. Phys. (Berlin) **525**, 87 (2013).
[28] A. Husakou, S.-J. Im, and J. Herrmann, Phys. Rev. A **83**, 043839 (2011).
[29] A. Husakou, F. Kelkensberg, J. Herrmann, and M. J. J. Vrakking, Opt. Express **19**, 25346 (2011).
[30] M. F. Ciappina, S. S. Aćimović, T. Shaaran, J. Biegert, R. Quidant, and M. Lewenstein, Opt. Express **20**, 26261 (2012).
[31] M. F. Ciappina, J. Biegert, R. Quidant, and M. Lewenstein, Phys. Rev. A **85**, 033828 (2012).
[32] T. Shaaran, M. F. Ciappina, and M. Lewenstein, Phys. Rev. A **86**, 023408 (2012).
[33] M. F. Ciappina, J. A. Pérez-Hernández, T. Shaaran, J. Biegert, R. Quidant, and M. Lewenstein, Phys. Rev. A **86**, 023413 (2012).
[34] T. Shaaran, M. F. Ciappina, and M. Lewenstein, J. Mod. Opt. **59**, 1634 (2012).
[35] I. Yavuz, E. A. Bleda, Z. Altun, and T. Topcu, Phys. Rev. A **85**, 013416 (2012).
[36] J. A. Pérez-Hernández, M. F. Ciappina, M. Lewenstein, L. Roso, and A. Zaïr, Phys. Rev. Lett. **110**, 053001 (2013).
[37] I. Yavuz, Phys. Rev. A **87**, 053815 (2013).
[38] M. F. Ciappina, J. A. Pérez-Hernández, T. Shaaran, L. Roso, and M. Lewenstein, Phys. Rev. A **87**, 063833 (2013).
[39] T. Shaaran, M. F. Ciappina, R. Guichard, J. A. Pérez-Hernández, L. Roso, M. Arnold, T. Siegel, A. Zaïr, and M. Lewenstein, Phys. Rev. A **87**, 041402(R) (2013).
[40] M. F. Ciappina, T. Shaaran, and M. Lewenstein, Ann. Phys. **525**, 97 (2013).
[41] T. Shaaran, M. F. Ciappina, and M. Lewenstein, Phys. Rev. A **87**, 053415 (2013).
[42] M. F. Ciappina, T. Shaaran, R. Guichard, J. A. Pérez-Hernández, L. Roso, M. Arnold, T. Siegel, A. Zaïr, and M. Lewenstein, Las. Phys. Lett. **10**, 105302 (2013).
[43] M. F. Ciappina, J. A. Pérez-Hernández, T. Shaaran, M. Lewenstein, M. Krüger, and P. Hommelhoff, Phys. Rev. A **89**, 013409 (2014).
[44] M. F. Ciappina, J. A. Pérez-Hernández, T. Shaaran, and M. Lewenstein, Eur. Phys. J. D **68**, 172 (2014).
[45] M. F. Ciappina, J. A. Pérez-Hernández, and M. Lewenstein, Comput. Phys. Commun. **185**, 398 (2014).

[46] M. F. Ciappina, J. A. Pérez-Hernández, L. Roso, A. Zaïr, and M. Lewenstein, J. Phys.: Conf. Ser. **601**, 012001 (2015).
[47] A. Husakou and J. Herrmann, Phys. Rev. A **90**, 023831 (2014).
[48] H. Ebadi, Phys. Rev. A **89**, 053413 (2014).
[49] B. Fetić, K. Kalajdžić, and D. B. Milošević, Ann. Phys. **525**, 107 (2012).
[50] J. Luo, Y. Li, Z. Wang, Q. Zhang, and P. Lu, J. Phys. B **46**, 145602 (2013).
[51] L. Feng, M. Yuan, and T. Chu, Phys. Plasmas **20**, 122307 (2013).
[52] Z. Wang, P. Lan, J. Luo, L. He, Q. Zhang, and P. Lu, Phys. Rev. A **88**, 063838 (2013).
[53] J. Luo, Y. Li, Z. Wang, L. He, Q. Zhang, P. Lan, and P. Lu, Phys. Rev. A **89**, 023405 (2014).
[54] L. He, Z. Wang, Y. Li, Q. Zhang, P. Lan, and P. Lu, Phys. Rev. A **88**, 053404 (2013).
[55] C. Zhang, C. Lui, and Z. Xu, Phys. Rev. A **88**, 035805 (2013).
[56] J. Luo, Y. Li, Z. Wang, Q. Zhang, P. Lan, and P. Lu, J. Opt. Soc. Am. B **30**, 2469 (2013).
[57] X. Cao, S. Jiang, C. Yu, Y. Wang, L. Bai, and R. Lu, Opt. Express **22**, 26153 (2014).
[58] Z. Wang, L. He, J. Luo, P. Lan, and P. Lu, Opt. Express **22**, 25909 (2014).
[59] L. Feng and H. Liu, Phys. Plasmas **22**, 013107 (2015).
[60] C. Yu, Y. Wang, X. Cao, S. Jiang, and R. Lu, J. Phys. B **47**, 225602 (2014).
[61] I. Yavuz, Y. Tikman, and Z. Altun, Phys. Rev. A **92**, 023413 (2015).
[62] L. Feng, Phys. Rev. A **92**, 053832 (2015).
[63] M. F. Kling, P. von den Hoff, I. Znakovskaya, and R. de Vivie-Riedle, Phys. Chem. Chem. Phys. **15**, 9448 (2013).
[64] A. F. Oskooi, D. Roundy, M. Ibanescu, P. Bermel, J. Joannopoulos, and S. G. Johnson, Comput. Phys. Commun. **181**, 687 (2010).
[65] K. C. Kulander, F. H. Mies, and K. J. Schafer, Phys. Rev. A **53**, 2562 (1996).
[66] J. L. Krause, K. J. Schafer, and K. C. Kulander, Phys. Rev. A **45**, 4998 (1992).